Turbulence Characteristics of Finlet Treatments Applied for Trailing Edge Noise Reduction of a NACA 0012 Airfoil

Felix Gstrein*, Bin Zang†, Yannick D. Mayer‡ and Mahdi Azarpeyvand§
Faculty of Engineering, University of Bristol, United Kingdom, BS8 1TR

This study experimentally investigates the near-field flow characteristics associated with the capability for trailing edge noise reduction of a selected finlet surface treatment applied on a NACA 0012 airfoil. It continues from a previous study, in which a variation of finlet parameters was examined in order to establish a configuration optimal for trailing edge noise reduction. To identify the features of the turbulent boundary layer that are directly related to the reduction of far-field noise, the development of the turbulence in the boundary layer within and around the area treated with the finlets is analyzed and compared with the results for the untreated airfoil. The results for the velocity auto-correlation and the cross-correlation of pressure and velocity are examined to substantiate results from the static surface pressure, unsteady surface pressure fluctuations and boundary layer velocity along the airfoil chord and in particular within the treated area. Upon further analysis of the pressure and velocity fields, it is demonstrated how the noise emission is reduced due to the decreased level of small-scale turbulence convected past the sharp trailing edge along the airfoil surface. The reduction is found to be likely the effect of an interaction between the flow channeled through the finlet treatment and coherent structures further away from the airfoil surface occurring at the trailing edge, but also surface friction along the finlet wall-structures.

I. Nomenclature

c	=	airfoil chord length (mm)
h	=	nozzle height (mm)
h_F	=	maximum finlet height (mm)
l	=	airfoil span length (mm)
p_0	=	reference pressure (µPa)
p'_{rms}	=	root-mean-square of pressure fluctuations (Pa)
Re	=	Reynolds number
R_{up}	=	pressure-velocity cross-correlation coefficient
U_e	=	irrotational flow velocity outside the boundary layer (m s^{-1})
U_∞	=	free-stream velocity (m s^{-1})
x, y, z	=	airfoil coordinate system (mm)
x_F, y_F	=	finlet coordinate system (mm)
α	=	geometric angle of attack (°)
α_e	=	effective angle of attack (°)
$\delta_{0.95}$	=	boundary layer thickness (mm)
η_F	=	local finlet height (mm)
τ	=	time lag (s)
ϕ_{uu}	=	velocity power spectral density (dB Hz^{-1})

*PhD Researcher, Mechanical Engineering, felix.gstrein@bristol.ac.uk.
†Lecturer, Aerospace Engineering, nick.zang@bristol.ac.uk.
‡Honorary Research Associate, Aerospace Engineering, yannick.mayer@bristol.ac.uk.
§Professor of Aerodynamics and Aeroacoustics, m.azarpeyvand@bristol.ac.uk.

II. Introduction

The development of airfoil trailing edge noise is a result of convected turbulence interacting with the sharp airfoil trailing edge [1, 2]. This process was mathematically formulated by Amiet [3], revealing that the noise emission to the far-field is dependent on the unsteady surface pressure fluctuations and the spanwise correlation length of the turbulence structures in the boundary layer at the airfoil trailing edge. Thus, if both, measurements of the sound pressure level (SPL) in the far-field and the unsteady surface pressure fluctuations are available, they can be compared in the frequency domain to relate modifications of the flow characteristics on the airfoil surface to changes in far-field noise. Furthermore, a detailed analysis of the boundary layer characteristics, including turbulence structures and their streamwise and spanwise correlation, is necessary to explain how systematical modifications of the flow in the boundary layer of an airfoil can reduce the far-field noise.

Since trailing edge noise is among the most dominant noise contributors from the airframe of aircraft [4], which is on the same emission intensity level as engine noise [4, 5], a large number of studies focus on the reduction or attenuation of the unsteady surface pressure fluctuations near the trailing edge as an effective measure to reduce the emitted noise. Approaches to a reduction of far-field noise by systematical modifications of the boundary layer can be classified as either active or passive noise control strategies. The most prominent active strategies, which all require additional energy to alter the boundary layer characteristics, are boundary layer injection [6, 7] and suction [8, 9]. A number of passive noise control strategies have been developed and applied to successfully reduce the noise emission of airfoils without additional energy input. These are mainly inspired by silently flying owl species, which have various features on their bodies and wings that contribute to the attenuation of the aerodynamic noise during their flight [10]. For a reduction of trailing edge noise, the most important approaches are trailing edge serrations [11–13], trailing edge brushes [14], porous materials [15–17] and finlet treatments [18–22].

In recent years, finlet treatments have gained increasing attention due to their capability to reduce trailing edge noise over a wide range of frequencies. Yet, the mechanisms leading to such significant noise reduction has not been fully understood. Finlets were first introduced by Clark et al. [19] as an attempt to reproduce the features of downy hairs on the surface of owl's feathers. They consist of thin, wall-like structures oriented in streamwise direction parallel to each other. After Clark et al. [19] had confirmed the noise reduction capabilities of finlets when applied flush with the trailing edge of a DU96-W180 airfoil, Afshari et al. [20] investigated finlet treatments applied upstream of the trailing edge of a flat plate. In doing so, they observed a dissipation effect as turbulence is "channeled" by the finlet treatments if the spacing between them is sufficiently large. Thereby, turbulence energy is assumed to be dissipated due to the increased surface area, added to the system through the finlet wall-structures. Moreover, they identified a shear layer building on top of the finlet treatments which eventually detaches at their ends. Later, Afshari et al. [21] also considered "3d finlets" for their tests on a flat plate by adding a staggered row of finlet wall-structures to the conventional treatment. They found that the emergence of a free shear layer in the finlet wake may be mitigated through a "third dimension" added to the conventional finlet treatments. Recently, Bodling and Sharma [22] performed a numerical investigation on finlets applied flush with the trailing edge of a NACA 0012 airfoil. They identified a reduction of surface pressure fluctuations at the trailing edge at frequencies above 2000 Hz as well as an increase at frequencies below and associated these observations with a lifting effect, moving turbulent eddies away from the airfoil surface as they are convected past the trailing edge. An attempt to identify and associate both, the channeling and dissipation effect described by Afshari et al. [20] and the lifting effect defined by Bodling and Sharma [22], was performed by Gstrein et al. [18]. They applied finlet treatments upstream of the trailing edge of a NACA 0012 airfoil and experimentally investigated the modifications to the boundary layer due to the presence of finlets. They observed an increase of the unsteady surface pressure fluctuations at frequencies lower than 1000 Hz at the trailing edge along with a decrease of small-scale turbulence (i.e. at higher frequencies). Gstrein et al. [18] related their observation with a detachment of turbulence structures from the airfoil surface and an emerging shear layer on top of the finlet treatments, as described by Afshari et al. [20].

In the previous study on finlet surface treatments applied on a NACA 0012 airfoil, Gstrein et al. [18] established finlet parameters optimal for the reduction of trailing edge noise. The right choice of the parameter set was found to be dependent on the boundary layer thickness near the trailing edge of the untreated airfoil. From the results of the static surface pressure, unsteady surface pressure fluctuations and velocity fluctuations in the boundary layer, they further observed a detachment of turbulence structures from the airfoil surface, which was identified as the main contributor to the reduction of trailing edge noise. Using experimental data describing the velocity auto-correlation and pressure-velocity cross-correlation, the present study focuses on the development of turbulence structures when a particular finlet treatment is applied on the NACA 0012 airfoil, which has been found to successfully reduce the trailing edge noise [18]. In doing so, the aim is to demonstrate how the varying distance of the convected turbulence structure

from the airfoil surface develops along the chord and thus to provide a better idea on the actual physics responsible for the reduction of trailing edge noise.

This paper continues the studies of Gstrein et al. [18] in order to investigate more thoroughly the process of turbulence detachment due to finlets and shed more light on the related trailing edge noise reduction mechanism. The experimental set-up as well as the measurement techniques applied in the experiments are detailed in Section III. In Section IV, the results are discussed, starting with the far-field sound pressure level for the treated and the untreated configuration. Subsequently, the power spectral density of the velocity and the pressure-velocity cross-correlations are presented and discussed. Concluding remarks are given in Section V.

III. Experimental Set-up

In the following, the experimental set-up, data collection, and analysis methods used to obtain the results presented in Section IV are explained. First, the facility is introduced, followed by a basic description of the applied measuring instruments and related calibration procedures. Then, the NACA 0012 airfoil model is presented together with its instrumentation. Finally, the design and dimensions of the applied finlet treatment are detailed.

A. Facility and Data Acquisition

The experiments were performed in the aeroacoustic facility of the University of Bristol, an open-jet test section anechoic above 160 Hz, connected to a temperature-controlled closed-circuit wind tunnel. With the mounted rectangular nozzle of width $l = 500\,\mathrm{mm}$ and height $h = 775\,\mathrm{mm}$, uniform flow speeds from $10\,\mathrm{m\,s^{-1}}$ to $40\,\mathrm{m\,s^{-1}}$ can be reached. A detailed description of the facility is provided by Mayer et al. [23].

The noise radiated from the airfoil trailing edge into the far-field was recorded using a portable beamforming array. The beamforming array was mounted above the airfoil and aligned with the center of the airfoil trailing edge at a vertical distance of 1 m. A delay-and-sum approach was applied to identify the contribution of trailing edge noise from the the far-field sound pressure contour using the Acoular software introduced by Sarradj and Herold [24]. The root-mean-square of the sound pressure fluctuations, p'_{rms}, was determined for one-third octave frequency bands with various center frequencies. Using the reference pressure $p_0 = 20\,\mu\mathrm{Pa}$, the sound pressure level (SPL) of the trailing edge noise is presented as $\mathrm{SPL} = 20\log_{10}\left(p'_{\mathrm{rms}}/p_0\right)$. The spectra were calculated using a Hanning window and 2^{12} samples per fast Fourier transform block with 50 % overlap. To restrict the recorded data to trailing edge noise only, the SPL determined for the distinct center frequencies were averaged over the area containing the focus of the trailing edge noise emission, as demonstrated in [18]. The beamforming array consists of a circular Aluminium plate about 850 mm in diameter, equipped with 64 Panasonic WM-61 A microphones, which are arranged along 9 spiral arms. The exact distribution of the microphones in the standard assembly and further details on the beamforming array are discussed by Mayer et al. [25]. The beamforming results used for evaluating the SPL were determined to be reliable for center frequencies between 500 Hz and 4000 Hz, where the uncertainty of the Panasonic microphones is 1.5 dB for a 95 % confidence interval [26].

Unsteady surface pressure data were measured using Knowles FG-23629-P16 pressure transducers mounted beneath pinholes 0.4 mm in diameter along the chord of the NACA 0012 airfoil to prevent pressure attenuation effects through a reduction of the sensing area of the transducers [27]. Furthermore, Panasonic WM-61A microphones were applied close to the trailing edge of the airfoil in a remote sensing configuration, which is detailed by Elsahar et al. [28]. Prior to performing the experiments, all microphones mounted on the airfoil and the beamforming array were calibrated against a G.R.A.S. 40PL reference microphone, which itself had been calibrated beforehand using a G.R.A.S. 42AA pistonphone. The described calibration procedure is the same as applied in previous studies [6, 16, 18].

The velocity was measured simultaneously with the surface pressure fluctuations to facilitate the calculation of the pressure-velocity cross-correlation. Thereby, a Dantec 55P15 hot-wire boundary layer probe was used, operated by a Dantec Streamline Pro system with a CTA91C10 module. The probe was calibrated using a Dantec 54H10 calibrator prior to performing the measurements. For the simultaneous measurement of surface pressure fluctuations and velocity a sampling rate of 2^{15} Hz was applied over a duration of 16 s for each run with a different position of the hot-wire probe. To obtain the velocity power spectral density (PSD), ϕ_{uu}, Welch's method was applied using a Hamming window with a size of 2^{12} samples and 50 % overlap to obtain the interim result u'^2_{rms}, which was subsequently transformed to $\phi_{uu} = 10\log_{10}\left(u'^2_{\mathrm{rms}}/U^2_\infty\right)$.

B. Airfoil and Instrumentation

The NACA 0012 airfoil considered for the tests has a span length of $l = 500\,\text{mm}$ and a chord length of $c = 300\,\text{mm}$. It was installed in a horizontal distance of 255.5 mm from the nozzle orifice between two side walls, which were attached to the frame to form an extension of the nozzle. The airfoil center line was aligned with the vertical center of the nozzle orifice. A schematic of the airfoil treated with finlets, including sections of the side walls, is shown in Fig. 1. The global coordinate system x, y, and z is placed such that x describes the direction parallel to the undisturbed free stream, y is normal to the airfoil center line at 0° angle of attack and z designates the spanwise direction. Using the described global coordinate system (x, y, z), the position of the beamforming array can be stated as (300 mm, 1000 mm, 0 mm). At $x/c \approx 0.1$, 60° zig-zag turbulator tapes of 6 mm overall width and 0.5 mm thickness were applied on both sides of the airfoil to trip the flow into forming a turbulent boundary layer. The free-stream velocity was kept constant at $U_\infty = 20\,\text{m}\,\text{s}^{-1}$ for the present investigations, so that the chord-based Reynolds number was $Re = 400\,000$ for all measurements. To adjust the angle of attack, the side walls were equipped with turntables which were designed to tightly support the airfoil model and turn it around the pivot at quarter chord. Since flow deflection effects are present in an open jet, the geometric angle of attack, α, has been corrected in order to obtain comparable results. For this purpose, the correction proposed by Brooks et al. [29] was applied, which was also referred to in other investigations on similar configurations [15, 30]. In this way, the corrected angle of attack α_e was obtained as

$$\alpha_e = \frac{\alpha}{\eta}, \tag{1}$$

where

$$\eta = (1 + 2\sigma)^2 + \sqrt{12\sigma}, \tag{2}$$

and

$$\sigma = \frac{\pi^2}{48}\left(\frac{c}{h}\right)^2. \tag{3}$$

As mentioned in the previous section, the NACA 0012 airfoil used is equipped with a large number of Knowles FG-23629-P16 pressure transducers and Panasonic WM-61A microphones close to the trailing edge, where the airfoil is

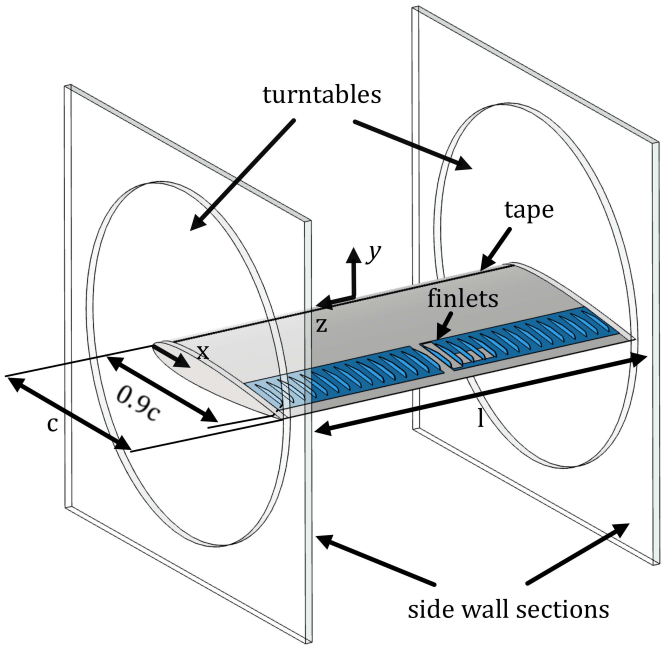

Fig. 1 Schematic of a NACA 0012 airfoil with side walls and a finlet treatment applied upstream of the trailing edge.

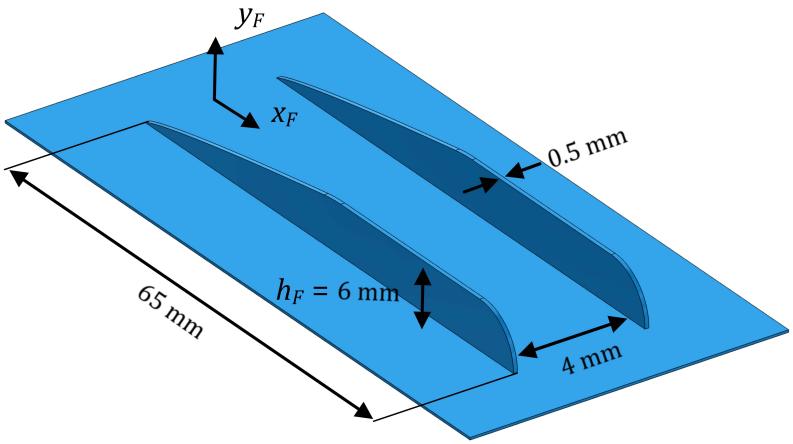

Fig. 2 Schematic of the finlet design including dimensions.

too thin to apply the Knowles transducers in a direct-sensing configuration (at $x/c \geq 0.95$). The complete description of the applied NACA 0012 airfoil and its instrumentation can be found in [31].

C. Finlet Design and Dimensions

The finlet treatment applied for the present investigations is based on the designs of Clark et al. [19] and Afshari et al. [20]. From the parameter studies performed in reference [18], one particular treatment was found to have optimal results for the considered configurations and thus is used in this work to study more thoroughly its effects while modifying the boundary layer characteristics on the NACA 0012 airfoil. The design and relevant dimensions are given in Fig. 2. The finlet treatment consists of a 0.3 mm thick substrate layer from which 0.5 mm thick wall-structures, the finlets, protrude vertically. In order to facilitate the description of the design, Fig. 2 introduces a local coordinate system x_F, y_F, where x_F describes the direction of the mean flow in the boundary layer and y_F the direction toward which the wall-structures extend. At the finlet front at $x_F = 0$ mm, where the flow enters the treated area, the finlet profile is tapered and shaped using the formula

$$y_F = 3.51 \cdot x_F^{4/5}, \tag{4}$$

which is proportional to the development of the boundary layer thickness on a flat plate [32]. At the rear part, the finlet profile is rounded with a radius equal to its maximum height, h_F, to allow for a smooth flow transition. As indicated in Fig. 2, the total finlet length is 65 mm, the height 6 mm and the spacing between the wall-structures 4 mm. Oriented in streamwise direction, as shown in Fig. 1, a treatment was mounted on each, the pressure and the suction side of the airfoil such that the rear edge of the finlets was located at $0.9c$ and the entire span of the airfoil was covered. Thereby, the substrate layer conformed to the slight curvature of the airfoil profile. It is further shown in Fig. 1 how the substrate layer has been locally removed to uncover pressure transducers in between of the finlets.

IV. Results

In this section, the experimental outcomes from reference [18] are further examined and elaborated using results from the velocity power spectral density, ϕ_{uu}, and the pressure-velocity cross-correlation coefficient, R_{up}, for the airfoil treated with the finlets and the untreated airfoil, referred to as baseline. To facilitate the association of boundary layer turbulence characteristics with the trailing edge noise emitted to the far-field, the results of the sound pressure level (SPL) for the treated and the baseline configuration are presented again. Previous experimental outcomes from reference [18] will also be used for the following discussions wherever a comparison is appropriate.

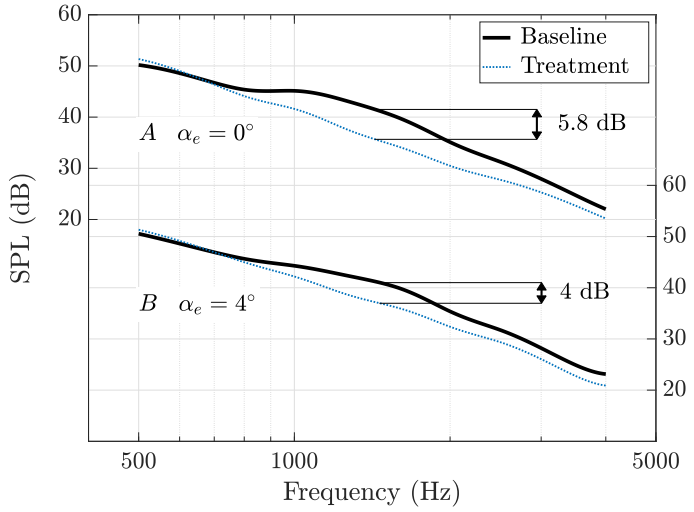

Fig. 3 Far-field SPL for the baseline and the treated configuration at the two angles of attack $\alpha_e = 0°$ and $\alpha_e = 4°$.

A. Sound Pressure Level from Trailing Edge Noise

Figure 3 shows the sound pressure level of the trailing edge noise in the far-field for the baseline and the treated configuration at the two different angles of attack, $\alpha_e = 0°$ and $4°$. With the flow remaining attached to the airfoil surface [33], the considered angles lie within the optimum application range of the introduced finlet treatment at the given Reynolds number and represent the zero and a positive lift configuration of the NACA 0012 airfoil. It can be observed that the introduced finlet treatment reduces the trailing edge noise at frequencies higher than 700 Hz, with a maximum reduction near 1400 Hz of 5.8 dB for $\alpha_e = 0°$ and 4 dB for $\alpha_e = 4°$. At frequencies lower than 700 Hz, the SPL for the treated configurations at both angles of attack considered slightly surpass the baseline, where the difference is within the uncertainty of the beamforming microphones.

B. Velocity Auto-correlations

To examine the boundary layer turbulence characteristics as a function of the airfoil surface distance along the y-direction (where $y = 0$ defines the airfoil surface here), the velocity power spectral density for the treated configuration is subtracted by the velocity PSD for the baseline to obtain the difference $\Delta\phi_{uu}$. Figure 4 shows the development of $\Delta\phi_{uu}$, depending on the distance, y, normalized by the maximum finlet height, h_F, and the frequency, from slightly upstream of the treated area toward the trailing edge at $\alpha_e = 4°$. Results for $\alpha_e = 0°$ show similar trends and are thus omitted for the sake of brevity. The boundary layer thickness for the treated configuration, $\delta_{0.95}$, is defined here as the distance along the y-axis where the velocity reaches 95 % of the irrotational flow outside the boundary layer edge, U_e, and is indicated in the contours of Fig. 4 with a dashed line. Furthermore, the measurement location with respect to the finlet-treated area is indicated with a black circle in the top-view. To facilitate the comparison with the unsteady surface pressure due to turbulence on the airfoil, representative results for the unsteady surface pressure PSD presented in reference [18] are shown in Fig. 5. As can be seen from Fig. 4a, the finlets increase $\Delta\phi_{uu}$ upstream of the treated area at $y/h_F \approx 1$ and above by approximately 4 dB Hz^{-1} at frequencies below 1000 Hz and a little further away from the airfoil surface at $y/h_F \approx 1.5$ at frequencies above 1000 Hz. Moving further downstream into the treated area, shown in Figs. 4b and 4c, the trend of a continuously decreasing $\Delta\phi_{uu}$ within the turbulent boundary layer becomes obvious, whereas $\Delta\phi_{uu}$ increases further below 1000 Hz at $y/h_F \approx 1.5$ and above 1000 Hz at $y/h_F \approx 2$. A more drastic effect of finlets can be observed at the transition from the treated area into the finlet wake, as shown in Fig. 4d. A reduction of the velocity fluctuation PSD is observed within the region of the boundary layer which is lower than the maximum finlet height within a frequency range between 100 Hz and 1000 Hz. Furthermore, $\Delta\phi_{uu}$ decreases sharply below $y/h_F = 0.5$ at frequencies higher than 5000 Hz. The low-frequency increase at $y/h_F \approx 1.5$ on the other hand is less intense than further upstream. Within the frequency range between 1000 Hz and 5000 Hz, there is a local increase in $\Delta\phi_{uu}$ close to the airfoil surface. The highly positive values for $\Delta\phi_{uu}$ at low frequencies upstream of and within the treated area

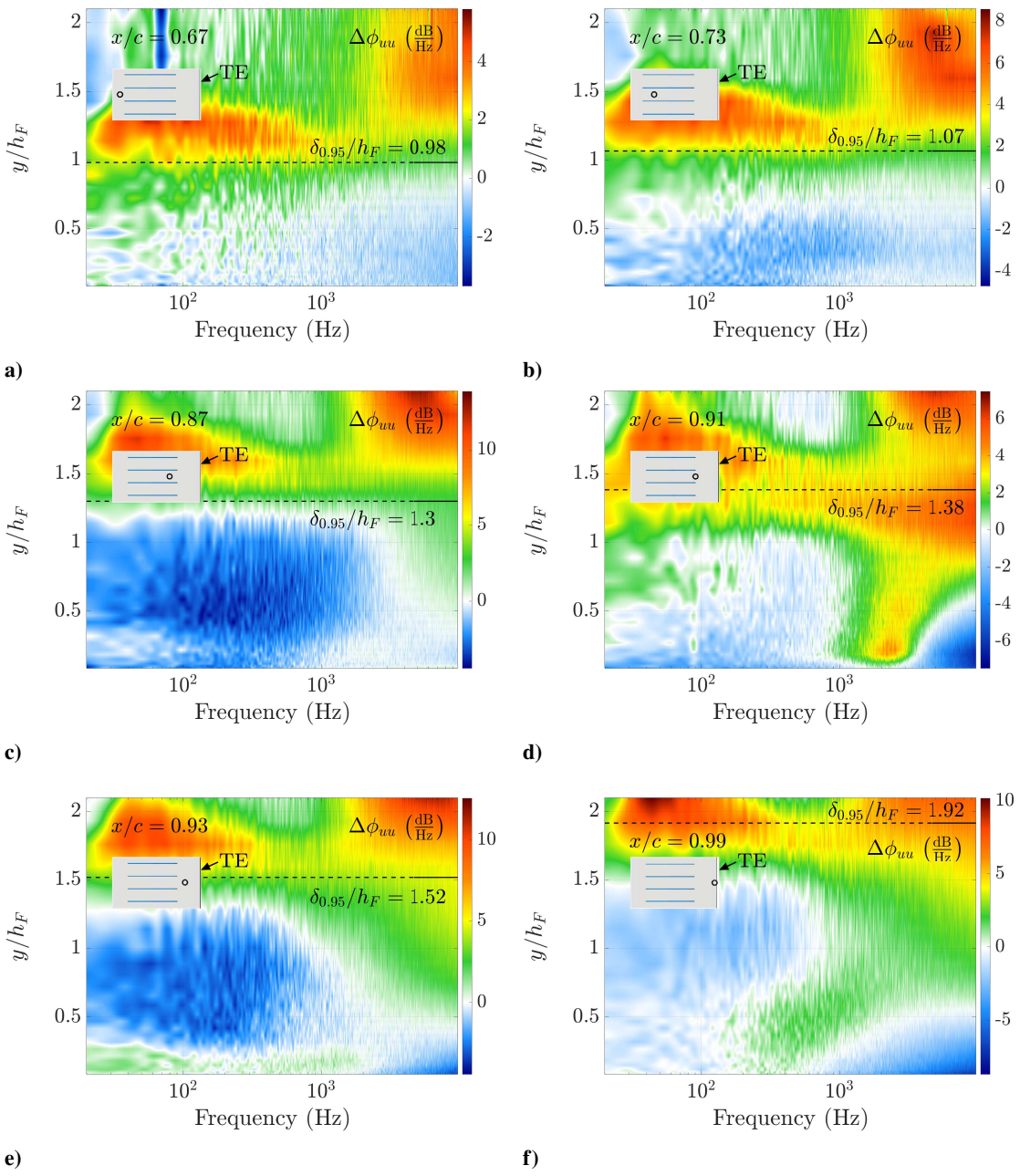

Fig. 4 Velocity fluctuation PSD difference between the treated NACA 0012 airfoil and its baseline configuration at $\alpha_e = 4°$ at various positions along the chord: a) $x/c = 0.67$, b) $x/c = 0.73$, c) $x/c = 0.87$, d) $x/c = 0.91$, e) $x/c = 0.93$, and f) $x/c = 0.99$.

suggest the formation of rather large coherent structures, agreeing with the results for the unsteady surface pressure PSD shown in Figs. 5a and 5b. From $x/c = 0.67$ to $x/c = 0.87$, the boundary layer thickness on the treated airfoil grows from $\delta_{0.95}/h_F = 0.98$ to $\delta_{0.95}/h_F = 1.3$, where the tapered leading edge part of the conventional finlets extends up to $\delta_{0.95}/h_F \approx 0.8$. With the growing boundary layer thickness, the $\Delta\phi_{uu}$ increase moves away from the airfoil surface as well. This observation and the continuously decreasing velocity fluctuation PSD within the tapered section of the finlets suggest that the coherent structures are a direct consequence of the interaction between the flow and the finlet leading edges. Toward the end of the treated area and the finlet trailing edges, the strictly negative values for $\Delta\phi_{uu}$ within and

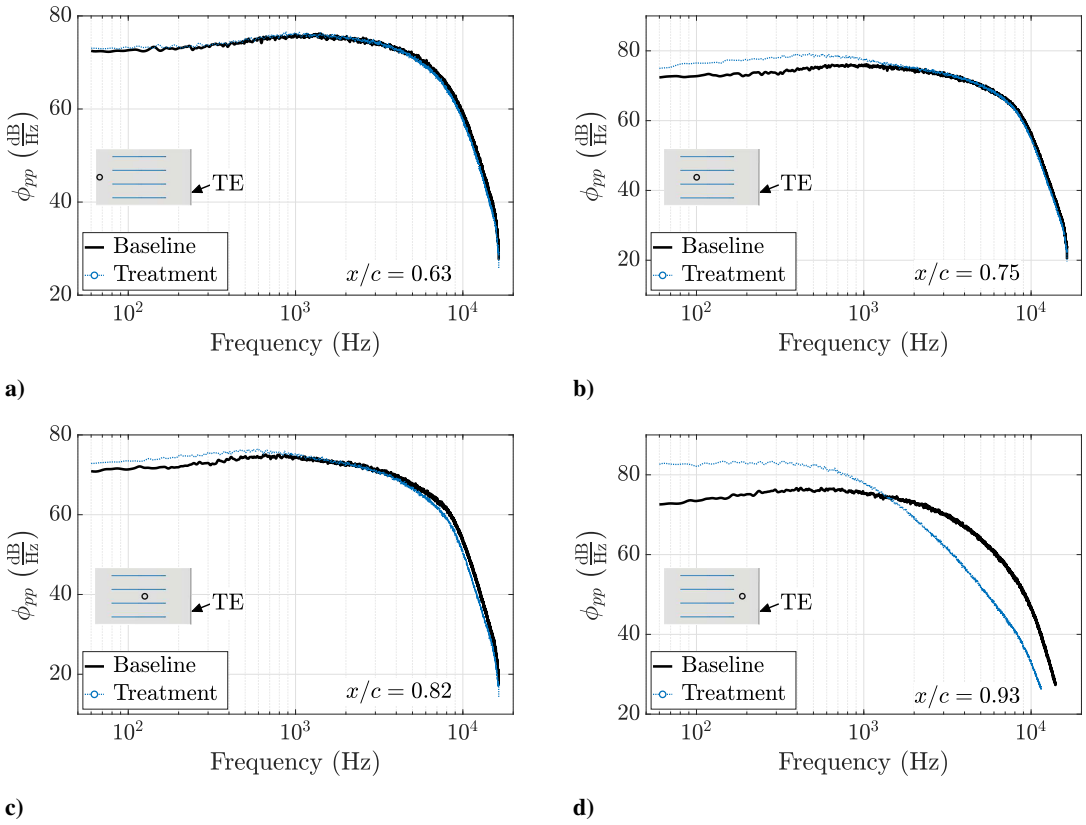

Fig. 5 Unsteady surface pressure fluctuation PSD results for the baseline and the treated configuration at $\alpha_e = 4°$, extracted from reference [18]: a) $x/c = 0.63$, b) $x/c = 0.75$, c) $x/c = 0.82$, and d) $x/c = 0.93$.

the positive values outside the boundary layer corroborate that the coherent structures form only around the ridge of the finlets and show that they develop further above the top of the treatments. This process together with wall friction effects might prevent turbulence structures to reach the airfoil surface, which will be examined more thoroughly in the next section. The pressure fluctuations originating from the larger structures on top of the finlets still propagate to the pressure transducers, as observed from the unsteady surface pressure PSD results from [18] shown in Fig. 5c. The increase of the velocity fluctuation PSD between 1000 Hz and 5000 Hz at $x/c = 0.91$ is likely due to vortices in the wake of each finlet wall-structure [20].

Figures 4e and 4f show the results for $\Delta\phi_{pp}$ in the section between the treated area and the trailing edge in the wake of the finlets. The data measured at these locations suggest that instead of lowering toward the airfoil surface, the structures that form and develop along the finlet ridges gain further vertical distance while convected downstream and past the trailing edge. Below the field of the convected coherent structures, the velocity fluctuation power spectral density for the treated airfoil further decreases, particularly at frequencies above 5000 Hz. The slightly increased values for $\Delta\phi_{uu}$ near the wall within the frequency range between 200 Hz and 500 Hz and from $y/h_F \approx 0.5$ upward at frequencies higher than 1000 Hz indicate that the structures forming at the trailing edges of the finlets are also convected toward the airfoil trailing edge. Hence, the effect of the reduced velocity fluctuation intensity likely is the result of friction effects along the finlet walls within the treated area and the mixing of distinct turbulence structures in the finlet wake.

Comparing the velocity fluctuation PSD from Figs. 4b and 4c with the surface pressure PSD for the same treatment presented in reference [18] as shown in Fig. 5b, it seems rather surprising that there is an increase of the low-frequency pressure fluctuation PSD within the front section of the treated area. However, it is possible [32] that the pressure fluctuations caused by the coherent structures at $y/h_F \approx 1.5$ propagate through the boundary layer to reach the airfoil surface. Similarly, the results for the velocity PSD in the finlet wake also agree well with the surface pressure PSD from reference [18] shown in Fig. 5d, indicating a reduction of small-scale turbulence near the airfoil surface whereas

large-scale turbulence increases. To further associate the velocity with the unsteady surface pressure measurements and relate them to the development of coherent structures forming due to finlet application, the pressure-velocity cross-correlation coefficient will be discussed next.

C. Pressure-velocity Cross-correlations

Figures 6 and 7 show the results for the pressure-velocity cross-correlation coefficients, R_{up}, for two different velocity measurement locations, $x_i/c = 0.73$ and $x_i/c = 0.87$, within the treated area on the airfoil for $\alpha_e = 4°$. Since the results for $\alpha_e = 0°$ show the same trends, they are again omitted for the sake of brevity. The velocity fluctuation profiles at each location have been correlated with the unsteady surface pressure fluctuations at three different locations, designated with x_j/c as indicated in the figure captions, both upstream and downstream of x_i/c. Thereby, the unsteady surface pressure fluctuations have been measured within a range of time lags, τ. The locations x_i/c are indicated with red squares, whereas the locations x_j/c are designated with a black circle in the top view inset of the figures. The cross-correlation has been normalized by the pressure variance and the free-stream velocity, U_∞. Furthermore, the pressure-velocity cross-correlation coefficient is shown as a function of the non-dimensional time lag, $\tau U_\infty/c$, and the distance from the airfoil surface, y, normalized by the local finlet height, $\eta_F(x_i)$. Figure 6 compares R_{up} for the baseline with the treated configuration in the front section of the finlet-treated area. In Figs. 6a and 6b, the correlation between the velocity fluctuations at $x_i/c = 0.73$ and the pressure fluctuations at $x_j/c = 0.72$ for the baseline and the treated configuration, respectively, are compared to each other. The results for the baseline configuration from Fig. 6a show a clear, positive correlation maximum of the unsteady surface pressure with the velocity fluctuations at a negative time lag, τ, and $y/\eta_F \approx 0$. In contrast, the maximum correlation for the treated configuration is observed close to $y/\eta_F = 1$ and at a negative time lag, τ, of larger magnitude. The surface pressure fluctuations at $x_j/c = 0.72$ on the treated airfoil are thus clearly associated with the velocity fluctuations originating from the ridge of the finlets at that location. Following the convected coherent structure further downstream along the airfoil chord, it can be observed from Figs. 6c and 6d as well as from Figs. 6e and 6f that at the other considered locations of the measured unsteady surface pressure fluctuations located downstream of the hot-wire position, the maximum correlation is found near the airfoil surface for the baseline and along the finlet ridges for the treated configuration. Moreover, the region of relatively large correlation compared to other time lags (i.e. with $R_{up} > 0.002$) is elongated across the boundary layer below the finlet height for the treated configuration and is oriented from smaller magnitudes of the time lag at high wall distances to larger magnitudes of the time lag at smaller wall distances. Hence, the pressure fluctuations further downstream are mainly correlated with the upstream velocity fluctuations originating at the finlet ridges. However, the elongated shape of the region with relatively large correlation (i.e. with $R_{up} > 0.0005$ in Fig. 6b and $R_{up} > 0.002$ in Figs. 6d and 6f), occurring for all results for the treated configuration, suggests that the surface pressure fluctuations also correlate with velocity fluctuations closer to the airfoil surface, which are likely the result of the interaction of the flow with the finlet leading edge and thus distributed within the boundary layer across the entire (local or maximum) finlet height. Furthermore, the tilted shape of the region of relatively high correlation (i.e. with values for R_{up} as detailed above) indicates that the lower structures forming at the very front of the treated area, and thus the finlet leading edge, travel more slowly than the structures above. This suggests that the coherent structures channeled through the finlet wall-structures are convected downstream with a lower speed than those originating along the finlet ridges, likely due to finlet-induced wall friction effects. The maximum of the cross-correlation coefficient decreases as a consequence of finlet application, suggesting that the turbulence is more distributed across the boundary layer for the treated configuration than for the baseline.

Figure 7 shows the pressure-velocity cross-correlation coefficient within the rear section of the finlet treated area, with $x_i/c = 0.87$. For the baseline, the maximum correlation between the unsteady surface pressure and velocity fluctuations at approximately the same location, $x_j \approx x_i$, is immediately on the airfoil surface, as shown in Fig. 7c. The pressure-velocity correlations determined with the unsteady surface pressure fluctuations from up- and downstream of x_i, shown in Figs. 7a and 7d, respectively, have their maximum correlation centers at slightly higher values of y/η_F, which likely reflects the airfoil curvature. The region of high correlation is still clearly focused at lower y/η_F than for the treated configuration further upstream.

For the treated configuration, shown in Figs. 7b, 7d, and 7f, two main differences compared with the baseline can be observed. First, the magnitude of the cross-correlation coefficient for the treated configuration is lower than for the baseline. Second, the region of relatively high correlation (i.e. for values where $R_{up} > 0.002$) extends slightly further into the y-direction for the treated configuration, where the magnitude of the time lag within this region again is clearly smaller above $y/h_F = 1$ than below the finlet height. The decreased positive cross-correlation coefficient for the treated configuration is likely the consequence of the wider distribution of the coherent turbulence structure. The second

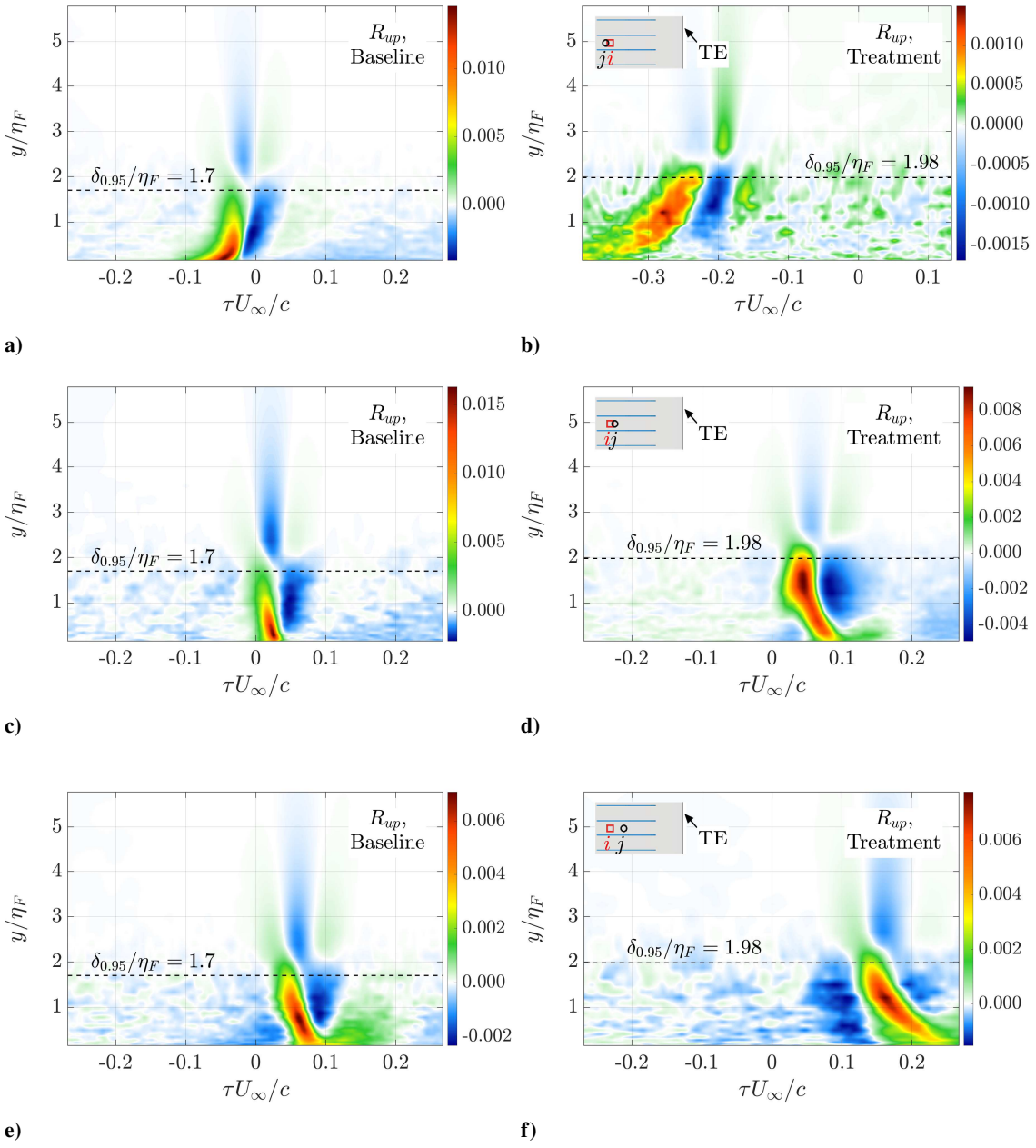

Fig. 6 Cross-correlation coefficients between the velocity fluctuations at $x_i/c = 0.73$ and the unsteady surface pressure fluctuations at x_j as functions of the airfoil surface distance and the time lag for the NACA 0012 airfoil at $\alpha_e = 4°$: a) baseline configuration with $x_j/c = 0.72$, b) treated configuration with $x_j/c = 0.72$, c) baseline configuration with $x_j/c = 0.75$, d) treated configuration with $x_j/c = 0.75$, e) baseline configuration with $x_j/c = 0.78$, and f) treated configuration with $x_j/c = 0.78$.

difference shows that in addition to the turbulence forming at the tapered finlet leading edges there are coherent structures on top of the treatment and that turbulence within the finlets is convected more slowly than the turbulence above the finlet wall-structures. Since the discussed region of relatively high values for the pressure-velocity cross-correlation lies within the (maximum) height of the finlets at a location further downstream of (and thus away from) the tapered finlet leading edges, it can be assumed that turbulence structures form only at the point of interaction between flow

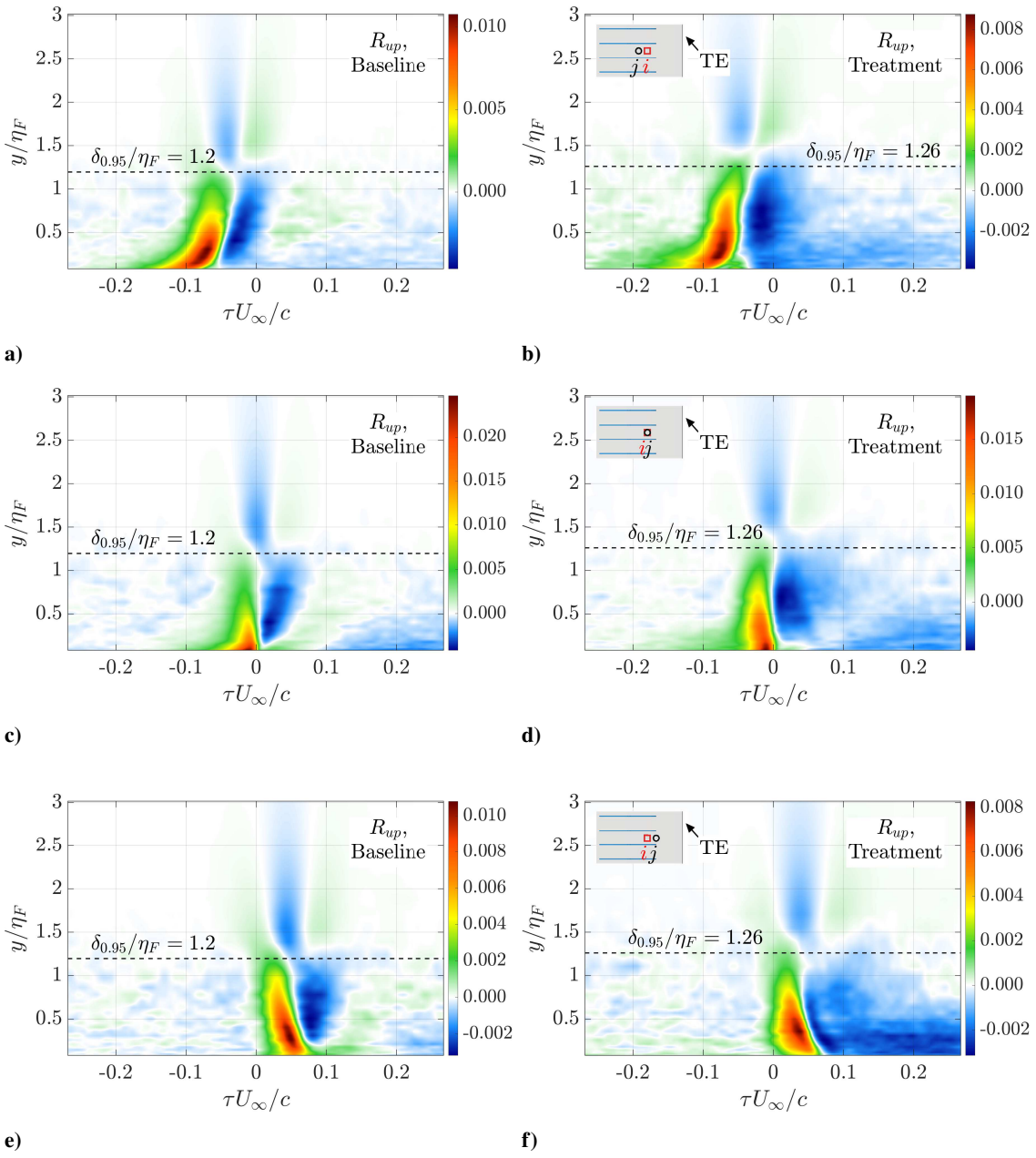

Fig. 7 Cross-correlation coefficients between the velocity fluctuations at $x_i/c = 0.87$ and the unsteady surface pressure fluctuations at x_j as functions of the airfoil surface distance and the time lag for the NACA 0012 airfoil at $\alpha_e = 4°$: a) baseline configuration with $x_j/c = 0.83$, b) treated configuration with $x_j/c = 0.83$, c) baseline configuration with $x_j/c = 0.87$, d) treated configuration with $x_j/c = 0.87$, e) baseline configuration with $x_j/c = 0.9$, and f) treated configuration with $x_j/c = 0.9$.

and finlet ridge, which is not distinguishable anymore further downstream. Hence, the correlation maximum at values above $y/\eta_F = 1$ are not only associated with lifting effects, but rather with turbulence generated along the tapered finlet leading edges.

To further investigate the changes of the turbulence characteristics near the trailing edge of the NACA 0012 airfoil due to finlet application, Figs. 8 and 9 show the pressure-velocity cross-correlation coefficients downstream of the

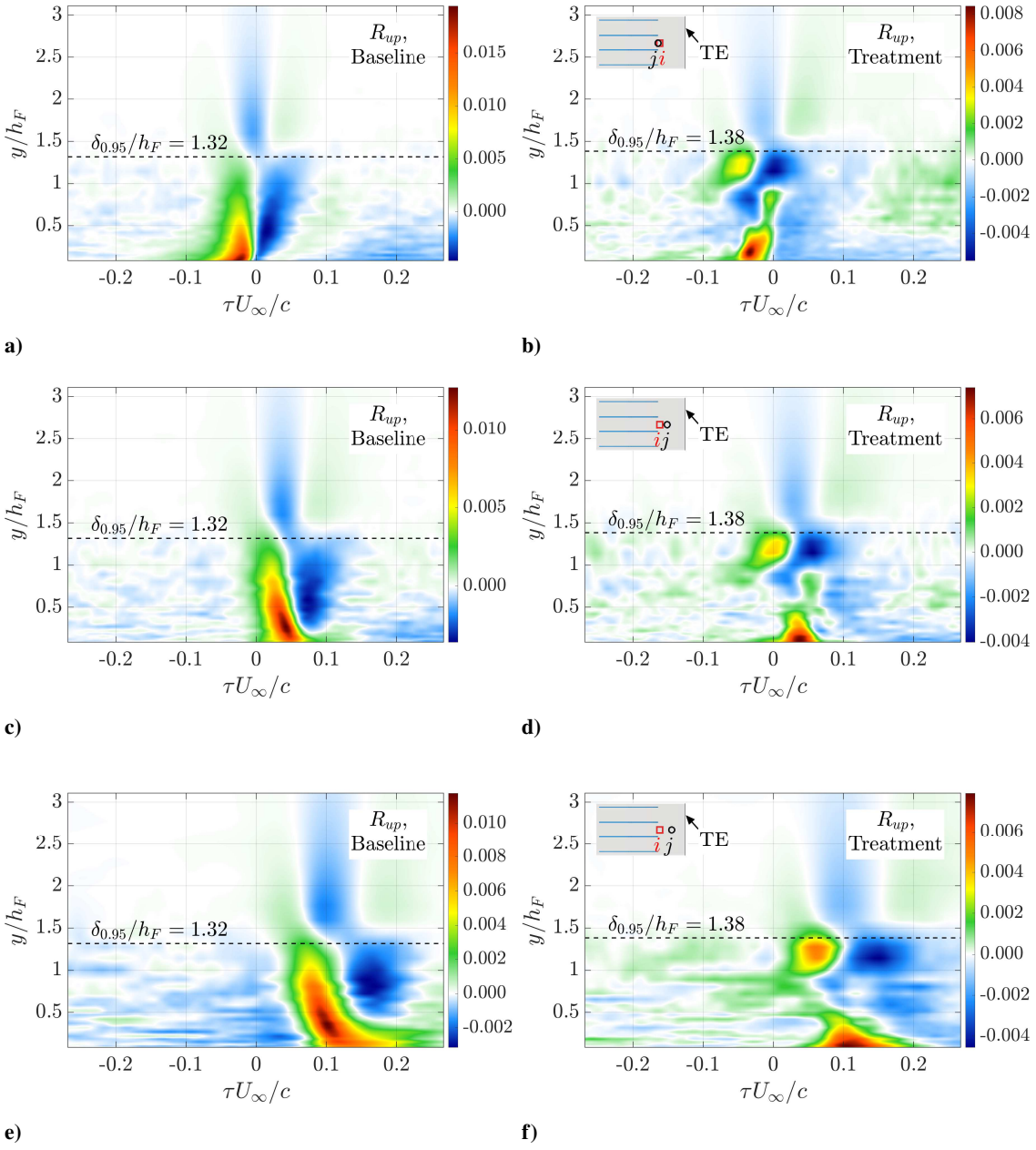

Fig. 8 Cross-correlation coefficients between the velocity fluctuations at x_i/c = 0.91 and the unsteady surface pressure fluctuations at x_j as functions of the airfoil surface distance and the time lag for the NACA 0012 airfoil at α_e = 4°: a) baseline configuration with x_j/c = 0.9, b) treated configuration with x_j/c = 0.9, c) baseline configuration with x_j/c = 0.93, d) treated configuration with x_j/c = 0.93, e) baseline configuration with x_j/c = 0.95, and f) treated configuration with x_j/c = 0.95,

treated area. Since the local finlet height is zero at these locations, the maximum finlet height, h_F, is used to normalize the distance of the airfoil surface, y. Figure 8 reflects the results for R_{up} immediately downstream of the treated area at $x_i/c = 0.91$, again comparing the treated configuration with the baseline for three different locations for the measured unsteady surface pressure fluctuations, designated as x_j/c. The results for the baseline, shown in Figs. 8a, 8c, and 8e, have trends similar to the upstream measurements. For the treated configuration on the other hand, shown in Figs. 8b,

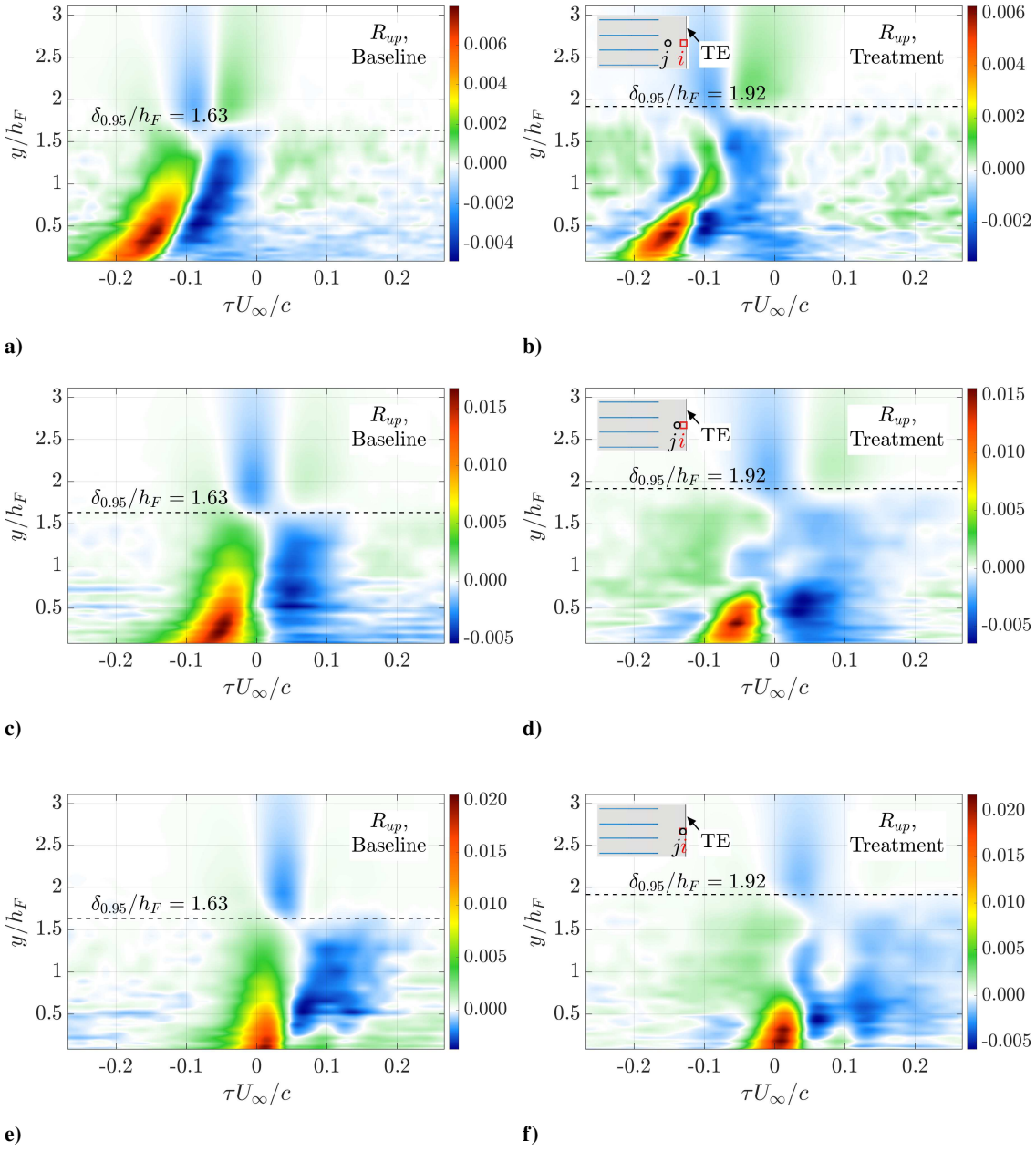

Fig. 9 Cross-correlation coefficients between the velocity fluctuations at $x_i/c = 0.97$ and the unsteady surface pressure fluctuations at x_j as functions of the airfoil surface distance and the time lag for the NACA 0012 airfoil at $\alpha_e = 4°$: a) baseline configuration with $x_j/c = 0.93$, b) treated configuration with $x_j/c = 0.93$, c) baseline configuration with $x_j/c = 0.97$, d) treated configuration with $x_j/c = 0.97$, e) baseline configuration with $x_j/c = 0.99$, and f) treated configuration with $x_j/c = 0.99$,

8d, and 8f, the distribution of R_{up} is different. The most evident feature is that there are now two local correlation maxima, one at the airfoil surface and another one at the maximum finlet height. It is clear that those two distinct structures have to be associated with the channeled flow and the coherent structures shed from the finlet trailing edges, which have already been observed from the velocity fluctuation PSD presented in the section above. The structures may be the direct result of a free shear layer that detaches from the finlet ridges at the trailing edges of the wall-structures

and has been reported by Afshari et al. [20]. Compared to the baseline, the magnitude of the correlation generally is lower, where the correlation values in the range between the coherent structure shed from the finlet trailing edge and the channeled turbulence are particularly low.

From the pressure-velocity cross-correlation results at the trailing edge, shown in Fig. 9, a minor local correlation maximum can be traced approximately at $y/h_F = 1.5$ for the treated configuration, likely representing the effect of the convected coherent structures shed at the finlet trailing edges. This observation agrees well with the results from the velocity fluctuation PSD discussed in the previous section, where a sharp increase for the treated configuration compared with the baseline has been observed above $y/h_F = 1.5$ near the trailing edge. From the weak correlation of unsteady surface pressure fluctuations with the velocity fluctuations at this height, it can be inferred that the coherent structures shed at the finlet trailing edges have a distance in the y-direction which is large enough to prevent them from interacting with the airfoil trailing edge and thus to contribute to trailing edge noise emission. These structures likely have a negligible momentum to move toward the airfoil surface after detaching from the finlets and their tendency to move further away is likely encouraged by the convex curvature of the airfoil profile. In contrast to the conditions within the treated area, the region of relatively high correlation to the coherent structure remaining close to the airfoil surface is smaller for the treated configuration than for the baseline. In particular, its extent along the y-direction is barely half of the expansion of the coherent structure for the baseline. It is possible that the turbulence structure further away from the airfoil surface interacts with the lower one in a way that the correlation to the latter decreases. The process of the decrease of the region of relatively high correlation (i.e. $R_{up} > 0.002$ in this case) can be observed from Fig. 9b, where the upper part of the lower coherent structure seems to be absorbed by the one above, possibly through viscous friction effects. Hence, it seems evident that the loss of correlation to turbulence in between of the channeled flow and the coherent structures shed at the rear ends of the finlets substantially contributes to the reduction of trailing edge noise.

V. Conclusions and Future Work

In the present study, the reduction of far-field trailing edge noise within the range of 700 Hz to 4000 Hz due to application of finlets on a NACA 0012 airfoil has been confirmed for two different angles of attack representing conditions without flow separation. Thereby, the maximum reduction has been found to reach 5.8 dB at a frequency of 1430 Hz for zero degree and 4 dB at a frequency of 1460 Hz for four degree of effective angle of attack. The findings of previous work in the field of finlet application on airfoils suggest that the noise reduction mechanism of finlet treatments applied on the NACA 0012 airfoil is associated with turbulence structures lifted away from the airfoil surface. From the present study's results for the velocity fluctuation power spectral density, coherent structures on top of the finlets have been identified and it has been shown that these structures continue to exist in the wake of the finlets and gain further height difference to the airfoil surface toward the trailing edge. It has been inferred from the pressure-velocity cross-correlations at different locations along the airfoil chord that coherent structures form along the tapered finlet leading edges due to the interaction between the flow and the wall-structures and that coherent structures are also shed from the rear edges of the finlets and convected toward the trailing edge. These turbulence structures have been found to rather be generated along the finlet ridges than being lifted from the airfoil surface, and hence the reduction of trailing edge noise due to finlets applied upstream of the trailing edge in a large part is likely due to the interaction of the turbulence shed from and the flow channeled through the finlet wall structures.

Acknowledgments

The authors would like to acknowledge the financial support of the EU H2020 ARTEM project under the grant agreement ID 769359.

References

[1] Glegg, S., and Devenport, W., *Aeroacoustics of Low Mach Number Flows*, Academic Press, 2017.

[2] Brooks, T. F., Pope, D., and Marcolini, M. A., "Airfoil self-noise and prediction," Reference Publication 1218, NASA, Langley Research Center, Hampton, Virginia, 1989.

[3] Amiet, R. K., "Noise due to turbulent flow past a trailing edge," *Journal of Sound and Vibration*, Vol. 47, No. 3, 1976, pp. 387–393. doi:10.1016/0022-460X(76)90948-2.

[4] Lilley, G. M., "The prediction of air frame noise and comparison with experiment," *Journal of Sound and Vibration*, Vol. 239, No. 4, 2001, pp. 849–859. doi:10.1006/jsvi.2000.3219.

[5] Lockard, D. P., and Lilley, G. M., "The airframe noise reduction challenge," Tech. mem. tm–2004–213013, NASA, Langley Research Center, Hampton, Virginia, 2004.

[6] Szőke, M., Fiscaletti, D., and Azarpeyvand, M., "Effect of inclined transverse jets on trailing-edge noise generation," *Physics of Fluids*, Vol. 30, No. 8, 085110, 2018. doi:10.1063/1.5044380.

[7] Leitch, T. A., Saunders, C. A., and Ng, W. F., "Reduction of unsteady stator-rotor interaction using trailing edge blowing," *Journal of Sound and Vibration*, Vol. 235, No. 2, 2000, pp. 235–245. doi:10.1006/jsvi.2000.2922.

[8] Szőke, M., Fiscaletti, D., and Azarpeyvand, M., "Influence of boundary layer flow suction on trailing edge noise generation," *Journal of Sound and Vibration*, Vol. 475, 11527, 2020. doi:10.1016/j.jsv.2020.115276.

[9] Wolf, A., Lutz, T., Würz, W., Krämer, E., Stalnov, O., and Seifert, A., "Trailing edge noise reduction of wind turbine blades by active flow control," *Wind Energy*, Vol. 18, No. 5, 2015, pp. 909–923. doi:10.1002/we.1737.

[10] Lilley, G. M., "A study of the silent flight of the owl," *4th AIAA/CEAS Aeroacoustics Conference*, AIAA 1998-2340, Toulouse, France, 1998, p. 2340. doi:10.2514/6.1998-2340.

[11] Azarpeyvand, M., Gruber, M., and Joseph, P. F., "An analytical investigation of trailing edge noise reduction using novel serrations," *19th AIAA/CEAS Aeroacoustics Conference*, AIAA 2013-2009, Berlin, Germany, 2013, p. 2009. doi: 10.2514/6.2013-2009.

[12] Mayer, Y. D., Lyu, B., Jawahar, H. K., and Azarpeyvand, M., "A semi-analytical noise prediction model for airfoils with serrated trailing edges," *Renewable Energy*, Vol. 143, 2019, pp. 679–691. doi:10.1016/j.renene.2019.04.132.

[13] Chong, T. P., and Vathylakis, A., "On the aeroacoustic and flow structures developed on a flat plate with a serrated sawtooth trailing edge," *Journal of Sound and Vibration*, Vol. 354, 2015, pp. 65–90. doi:10.1016/j.jsv.2015.05.019.

[14] Herr, M., and Dobrzynski, W., "Experimental investigations in low-noise trailing-edge design," *AIAA Journal*, Vol. 43, No. 6, 2005, pp. 1167–1175. doi:10.2514/1.11101.

[15] Geyer, T., Sarradj, E., and Fritzsche, C., "Measurement of the noise generation at the trailing edge of porous airfoils," *Experiments in Fluids*, Vol. 48, No. 2, 2010, pp. 291–308. doi:10.1007/s00348-009-0739-x.

[16] Ali, S. A. S., Azarpeyvand, M., and Da Silva, C. R. I., "Trailing-edge flow and noise control using porous treatments," *Journal of Fluid Mechanics*, Vol. 850, 2018, pp. 83–119. doi:10.1017/jfm.2018.430.

[17] Showkat Ali, S. A., Azarpeyvand, M., Szőke, M., and Ilário Da Silva, C. R., "Boundary layer flow interaction with a permeable wall," *Physics of Fluids*, Vol. 30, No. 8, 085111, 2018. doi:10.1063/1.5043276.

[18] Gstrein, F., Zang, B., and Azarpeyvand, M., "Application of Finlets for Trailing Edge Noise Reduction of a NACA 0012 Airfoil," *AIAA Aviation Forum*, AIAA 2020-2502, VIRTUAL EVENT, 2020, p. 2502. doi:10.2514/6.2020-2502.

[19] Clark, I. A., Alexander, W. N., Devenport, W., Glegg, S., Jaworski, J. W., Daly, C., and Peake, N., "Bioinspired trailing-edge noise control," *AIAA Journal*, Vol. 55, No. 3, 2017, pp. 740–754. doi:10.2514/1.J055243.

[20] Afshari, A., Azarpeyvand, M., Dehghan, A. A., Szöke, M., and Maryami, R., "Trailing-edge flow manipulation using streamwise finlets," *Journal of Fluid Mechanics*, Vol. 870, 2019, pp. 617–650. doi:10.1017/jfm.2019.249.

[21] Afshari, A., Dehghan, A. A., and Azarpeyvand, M., "Novel three-dimensional surface treatments for trailing-edge noise reduction," *AIAA Journal*, Vol. 57, No. 10, 2019, pp. 4527–4535. doi:10.2514/1.J058586.

[22] Bodling, A., and Sharma, A., "Numerical investigation of noise reduction mechanisms in a bio-inspired airfoil," *Journal of Sound and Vibration*, Vol. 453, 2019, pp. 314–327. doi:10.1016/j.jsv.2019.02.004.

[23] Mayer, Y. D., Jawahar, H. K., Szőke, M., Ali, S. A. S., and Azarpeyvand, M., "Design and performance of an aeroacoustic wind tunnel facility at the University of Bristol," *Applied Acoustics*, Vol. 155, 2019, pp. 358–370. doi:10.1016/j.apacoust.2019.06.005.

[24] Sarradj, E., and Herold, G., "A Python framework for microphone array data processing," *Applied Acoustics*, Vol. 116, 2017, pp. 50–58. doi:10.1016/j.apacoust.2016.09.015.

[25] Mayer, Y., Zang, B., and Azarpeyvand, M., "Design of a Kevlar-walled test section with dynamic turntable and aeroacoustic investigation of an oscillating airfoil," *25th AIAA/CEAS Aeroacoustics Conference*, AIAA 2019-2464, Delft, The Netherlands, 2019, p. 2464. doi:10.2514/6.2019-2464.

[26] Celik, A., Bowen, J. L., and Azarpeyvand, M., "Effect of trailing-edge bevel on the aeroacoustics of a flat-plate," *Physics of Fluids*, Vol. 32, No. 10, 2020, p. 105116. doi:10.1063/5.0024248.

[27] Gravante, S. P., Naguib, A. M., Wark, C. E., and Nagib, H. M., "Characterization of the pressure fluctuations under a fully developed turbulent boundary layer," *AIAA Journal*, Vol. 36, No. 10, 1998, pp. 1808–1816. doi:10.2514/2.296.

[28] Elsahhar, W., Showkat Ali, S. A., Theunissen, R., and Azarpeyvand, M., "An experimental investigation of the effect of bluff body bluntness factor on wake-vortex noise generation," *AIAA/CEAS Aeroacoustics Conference*, AIAA 2018-3288, Atlanta, Georgia, 2018. doi:10.2514/6.2018-3288.

[29] Brooks, T. F., Marcolini, M. A., and Pope, D. S., "Airfoil trailing edge flow measurements and comparisons with theory, incorporating open wind tunnel corrections." *9th AIAA/NASA Aeoracoustics Conference*, AIAA 1984-2266, Williamsburg, Virginia, USA, 1984, p. 2266. doi:10.2514/6.1984-2266.

[30] Hutcheson, F. V., and Brooks, T. F., "Effects of angle of attack and velocity on trailing edge noise determined using microphone array measurements," *International Journal of Aeroacoustics*, Vol. 5, No. 1, 2006, pp. 39–66. doi:10.1260/147547206775220425.

[31] Zang, B., Mayer, Y. D., and Azarpeyvand, M., "An experimental investigation on the mechanism of tollmien-schlichting waves for a naca 0012 aerofoil," *25th AIAA/CEAS Aeroacoustics Conference*, AIAA 2019-2609, Delft, The Netherlands, 2019, p. 2609. doi:10.2514/6.2019-2609.

[32] Schlichting, H., and Kestin, J., *Boundary-layer theory*, 7$^{\text{th}}$ ed., McGraw-Hill, New York, USA, 1979.

[33] Mayer, Y. D., Zang, B., and Azarpeyvand, M., "Aeroacoustic characteristics of a NACA 0012 airfoil for attached and stalled flow conditions," *25th AIAA/CEAS Aeroacoustics Conference*, AIAA 2019-2530, Delft, The Netherlands, 2019, p. 2530. doi:10.2514/6.2019-2530.